Available online at www.sciencedirect.com
SCIENCE DIRECT®
Chemical Physics Letters 400 (2004) 122–127
CHEMICAL PHYSICS LETTERS
www.elsevier.com/locate/cplett

# Investigation of Co nanoparticles with EXAFS and XANES

Guangjun Cheng [1], Joshua D. Carter, Ting Guo *

*Chemistry Department, University of California, One Shields Avenue, Davis, CA 95616, USA*

Received 5 August 2004; in final form 15 October 2004
Available online 11 November 2004

**Abstract**

3, 5, and 12-nm Co nanoparticles were synthesized via thermo-decomposition. Extended X-ray absorption fine structure (EXAFS) and X-ray absorption near-edge structure (XANES) were used to probe the structures of these nanoparticles. Simulations were carried out to compare the EXAFS profiles of three different crystalline phases of Co. The results of EXAFS and XANES suggested that the reactivity of these nanoparticles towards their environment is inversely proportional to their size. Sharp decreases in the amplitude of EXAFS of these nanoparticles were observed, which could be attributed to the existence of the disorder in those crystalline nanostructures.


## 1. Introduction

Nanoscale materials are of great importance because of their potential applications in electronics, optics, and catalysis [1,2]. The properties of these nanoscale materials can be expected to be between those of the bulk and isolated atoms. To exploit their full application potentials, it is important to thoroughly investigate the structural, electronic, magnetic and optical properties of these nanomaterials. Recently X-ray absorption spectroscopy (XAS), in particular extended X-ray absorption fine structure (EXAFS) and X-ray absorption near-edge structure (XANES), has been used as powerful tools for studying the structures and dynamics of the nanoscale materials [3–9].

EXAFS have been used extensively in the investigation of local atomic structures such as the number and type of neighboring atoms, inter-atomic distances, and disorder. Since the application of EXAFS does not require the materials to have a long-range order [10,11], it is well suited for determining the local structures of both non-crystalline and crystalline materials. A number of colloidal nanocrystals have been characterized by EXAFS and XANES, including CdS [12], CdSe [13], $SnO_2$ [14], Manganese oxides [15,16], $MoS_2$ [17], and Au [18,19].

The aim of this study is to characterize the structure and stability of as-prepared Co nanoparticles, and the outcome of which will be useful to in situ EXAFS measurements of these Co nanoparticle catalysts. We will describe the results of the synthesis and characterization of three different size Co nanoparticles using XAS, transmission electron microscopy (TEM), and atomic force microscopy (AFM). The X-ray absorption measurements were performed under both ambient and anaerobic conditions. Theoretical simulations were carried out to illustrate the effect of crystalline structures on EXAFS.

## 2. Experimental

Dicobalt octacarbonyl $Co_2(CO)_8$ containing 1–5% hexane stabilizer, oleic acid (OA, 99%), anhydrous *o*-dichlorobenzene (DCB, 99%), tri-octylamine (TOA,

* Corresponding author.
*E-mail address:* tguo@ucdavis.edu (T. Guo).
[1] Current address: Physics Laboratory, National Institute of Standards and Technology, Gaithersburg, MD 20899, USA.

0009-2614/$ - see front matter © 2004 Elsevier B.V. All rights reserved.
doi:10.1016/j.cplett.2004.10.095

98%), cobalt(II) oxide and boron nitride were purchased from Aldrich. Tri-octylphosphine oxide (TOPO, 90%) was purchased from Alfa Aesar. All chemicals were used without further treatment.

Co nanoparticles were synthesized using standard procedures [20,21]. In brief, TOPO was degassed in Ar in a three-neck flask for 20 min. A 15 mL OA in DCB solution was introduced into the flask under Ar. The solution was then heated to the reflux temperature of DCB (~182 °C). 0.54 g of $Co_2(CO)_8$ diluted in 3 mL of DCB was quickly injected into the refluxing solution. In order to obtain different sizes of Co nanoparticles, different combinations of surfactants were used. Typically, the combination of 0.1 mL OA, 0.9 mL TOA and 0.05 g TOPO was used to produce 3 nm nanoparticles; the combination of 0.2 mL OA and 0.1 g TOPO yielded 5 nm nanoparticles; and the combination of 0.1 mL OA and 0.2 g TOPO was used to make 12 nm nanoparticles.

Nanoparticle size, morphology, structure, and selected area diffraction (SAD) were probed using a Philips CM-12 TEM (100 kV). TEM samples were prepared by dropping the colloids solution onto carbon-coated TEM grids. AFM (Nanoscope IIIA, Digital Instruments) measurements operated in the tapping mode were performed to determine the size of 3-nm nanoparticles. AFM samples were prepared by immersing a Si wafer cleaned with Piranha solution (4:1 conc. $H_2SO_4$:$H_2O_2$ (30%)) into the 3-nm nanoparticle colloid solution for several minutes, followed by rinsing with toluene and drying with Ar gas.

EXAFS measurements were performed on the K edge of Co in Co nanoparticles and a 3-μm thick Co thin foil standard. Co nanoparticle samples were prepared under the ambient condition by directly dropping the colloid Co nanoparticle solutions onto Kapton tapes to form thin layers in air. Another set of Co nanoparticle samples were prepared using the same method of dropping and drying, but all the procedures were performed in a dry-box (<1 ppm oxygen and water). After dried in the dry-box, the samples were sealed with Kapton tapes, and then taken out of the dry-box. CoO sample was prepared by grinding with boron nitride and pressing into a pellet.

The experiments were performed at the beamline 4–1 at the Stanford Synchrotron Radiation Laboratory (SSRL) with a double silicon crystal (220) monochromator [5]. Harmonics were suppressed by detuning the crystal spectrometer. All the samples were measured at room temperature. EXAFS data were obtained by detecting the fluorescence of K lines from Co in Co nanoparticles using a Lytle detector. Simultaneously, transmission mode detected with ion chambers was employed to acquire the EXAFS data on the standard Co foil. In fluorescence mode, thin Mn foil filter placed in front of the Lytle detector was used to reduce the scattering of incident X-rays by the sample and sample holder. The EXAFS data were collected using the XAS program at SSRL.

EXAFS data analysis was performed using EXAFSPAK [22]. The subtraction of polynomial fit pre-edge and spline-fit atomic absorption curves, and $k^3$ factor multiplication were all built-in in the EXAFSPAK package. The processed EXAFS data in k reciprocal space was directly obtained from that in the energy space. The radial distribution function (RDF) in real space was then obtained via Fourier transformation of the EXAFS data in k space. A 1–5 Å range was used for displaying the RDFs.

## 3. EXAFS simulations

The EXAFS patterns for three different phases of Co bulk, face-centered cubic (fcc), hexagonal close packed (hcp) and epsilon-Co were simulated. For hcp Co, the program 'ATOMS' was used to generate the 'feff.inp' files, which were used for EXAFS simulation using FEFF8 [23,24]. The 'feff.inp' file provided a list of atomic coordinates in the crystal. For other two phases of Co, fcc and epsilon phase, the 'feff.inp' files were generated based on their X-ray crystallography data. For all the simulations, the Debye temperature and the measuring temperature were set to be 450 and 300 K, respectively. We assumed that Co nanoparticles had the same Debye temperature as the bulk.

The generated 'feff.inp' files were used in FEFF8 program, which calculated extended X-ray absorption fine structure (EXAFS) using an ab-initio self-consistent real space multiple scattering (RSMS) approach [23,24]. FEFF8 program generated a large number of scattering paths. All scattering paths shorter than 5.0 Å, including multiple scatterings, were used to simulate the EXAFS pattern. The OPT program in EXAFSPAK were used to treat all these scattering paths, which produced the simulated EXAFS results and their corresponding FFT patterns.

## 4. Results and discussions

We simulated the EXAFS patterns for three different crystalline phases of Co bulk: fcc, hcp and epsilon. For fcc and hcp Co bulk, there is only one type of Co atom in a unit cell, in which all the Co atoms have the same surrounding environments. However, there are two types of Co atoms in epsilon, which have different surrounding environments in a unit cell [25]. Thus, two 'feff.inp' files were generated for two types of Co atoms appearing in one unit cell.

Fig. 1a shows the EXAFS simulation results for two types of Co atoms. The total EXAFS for epsilon-Co and their corresponding FFT patterns are shown in Fig. 1b.

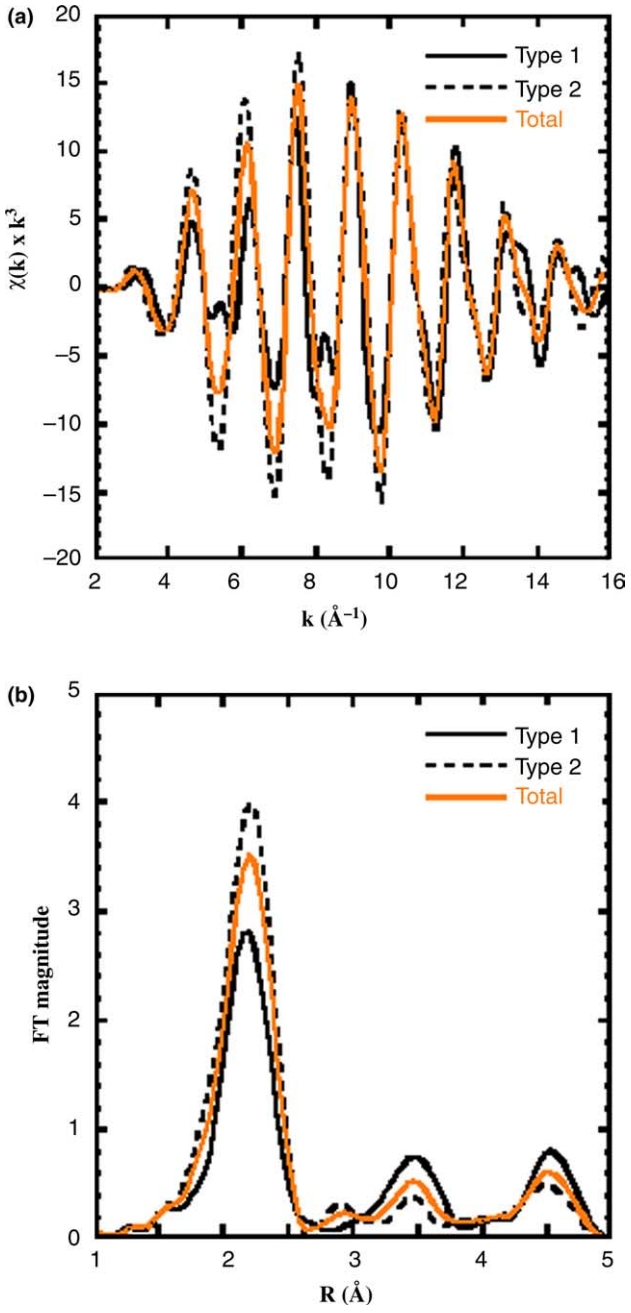


Fig. 1. Co K EXAFS simulations of two types of Co atoms in epsilon-Co and the epsilon-Co bulk (a), and the corresponding Fourier transforms (b).

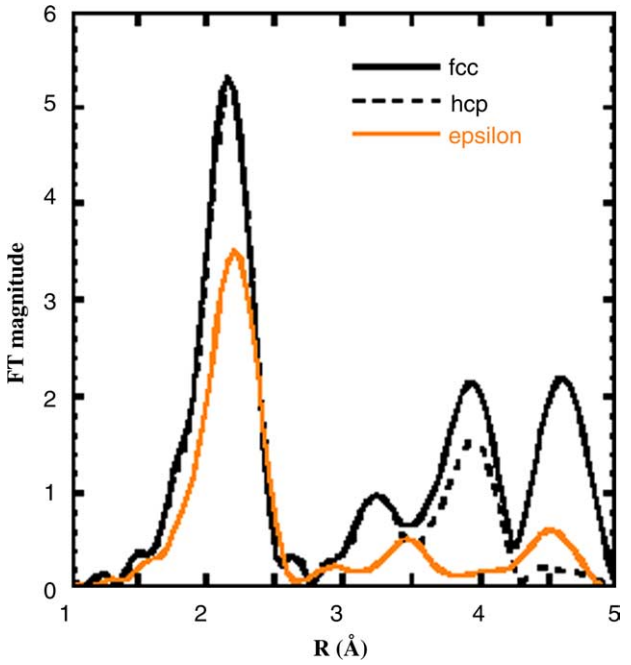


Fig. 2. Fourier transforms of three different phases of Co, fcc, hcp and epsilon.

The simulated FFT patterns from three different phases of Co bulk are shown in Fig. 2. From these simulations, it can be seen that the FFT patterns of fcc and hcp are similar in the first shell (2.0 Å) and the second shell (3.3 Å). The third peak (3.8 Å) in the hcp structure has a lower magnitude, and no obvious peak on the fourth shell for hcp-Co. However, the fourth peak (4.6 Å) is intense for fcc due to the multiple scattering. The FFT of epsilon-Co is much different from that of fcc-Co and hcp-Co. The magnitudes for all the peaks are lower due to the fact that the atoms in epsilon-Co are not closely packed. In addition, the peak positions for higher shells are different from those in fcc or hcp-Co. There are two peaks at 3.5 and 4.5 Å, which do not appear in fcc-Co or hcp-Co either. The two peaks around 3.2 and 3.8 Å in fcc-Co and hcp-Co do not show up in epsilon-Co. Therefore, EXAFS can be used to differentiate these three different phases of Co bulk, provided that the Co material under investigation has a well-defined crystalline structure.

Fig. 3a shows the TEM micrograph of 12-nm Co nanoparticles, and Fig. 3b shows the SAD pattern on this sample. It indicates that 12-nm Co nanoparticles adopt epsilon-Co. Fig. 3c shows the TEM micrograph of 5-nm Co nanoparticles. Although 12-nm Co nanoparticles give a clear electron diffraction pattern, which indicates that there is a long range ordering in it, 5- and 3-nm Co nanoparticles do not. This could be caused by the limited amount of samples in selected area or amorphous/crystalline mixture or oxidations of these small nanoparticles.

Because of the limitation of the resolution of the TEM used here, AFM was used to characterize 3-nm Co nanoparticles (Fig. 3d). The section analysis shown in Fig. 3e clearly shows that the average size of nanoparticle is ~3 nm.

Fig. 4a show normalized XANES spectra of as-prepared Co nanoparticles in an open-air environment at room temperature. XANES from a standard Co foil and CoO are also shown as the references. As shown in Fig. 4a, the XANES pattern of the 12-nm sample

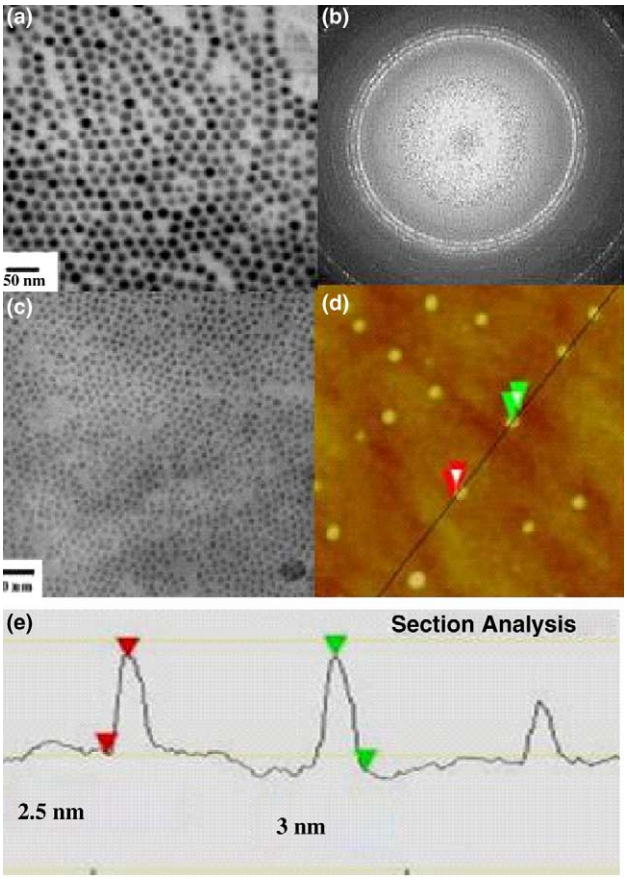


Fig. 3. TEM micrographs of 12-nm Co nanoparticles (a), 5-nm Co nanoparticles (c), and selected area diffraction pattern for 12-nm Co nanoparticles (b). AFM images for 3-nm Co nanoparticles (d) and its section analysis (e).

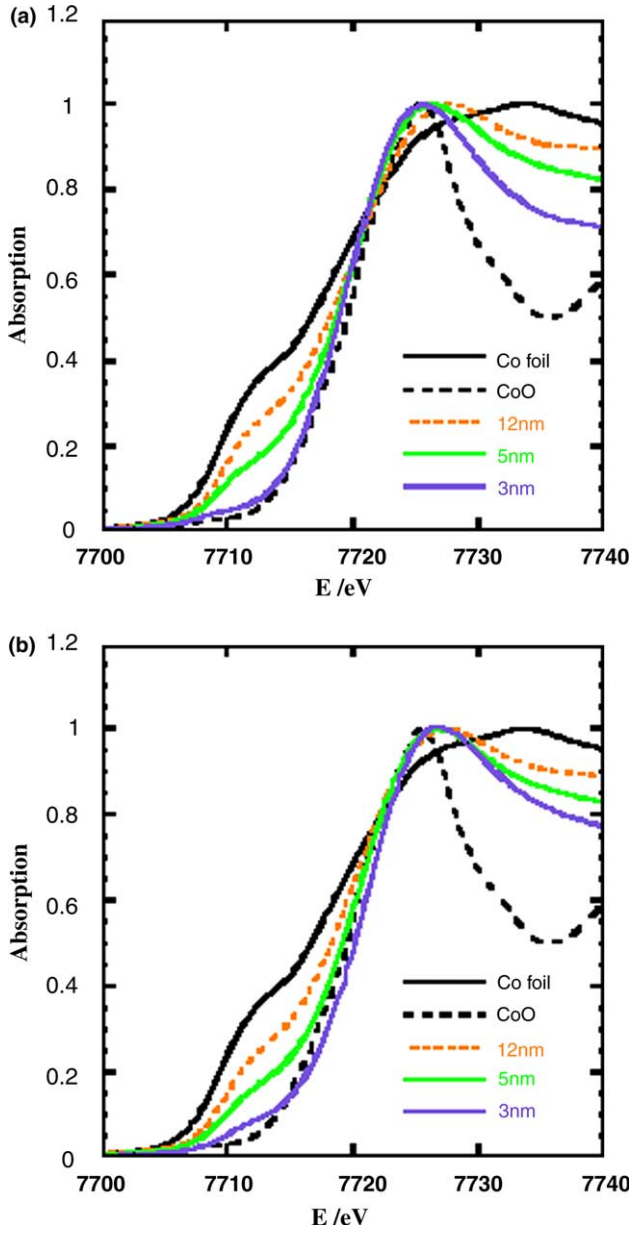


Fig. 4. Normalized XANES patterns for Co foil and 3, 5, 12-nm Co nanoparticles prepared under ambient conditions (a), and under anaerobic conditions (b).

resembles closely to that of the Co foil, which has a significant shoulder around 7712 eV. The XANES of 5-nm nanoparticles has a much smaller shoulder, and that of 3-nm nanoparticle shows almost no shoulder around 7712 eV. In the meantime, the patterns between 20 and 40 eV above the absorption edges of these three samples are all somewhat between that of Co bulk and CoO, with 12 nm nanoparticles closest to the bulk, and 3 nm particles closest to CoO. These results can be explained by the reactions of these nanoparticles with oxygen in the air to form oxides.

The XANES results for the Co nanoparticles prepared in the dry-box are shown in Fig. 4b. The 12-nm nanoparticles show the same result as the sample prepared in the open-air environment. Under protection, the XANES of 3- and 5-nm nanoparticles become slightly closer to that Co bulk in the XANES region 20–40 eV above the edge. Therefore, the preparation in dry-box protects both nanoparticles, to some extent. From Fig. 4, it is obvious that the XANES patterns of 3- and 5-nm are still far from being identical to that of CoO. Although the main component in those nanoparticles is oxygen around Co, as can be seen below in the EXAFS section, apparently these nanoparticles adopt different structures than CoO bulk, possibly due to the large portion of the atoms in the surface layer that are bonded to surfactants.

Fig. 5 shows the FFT of the experimental EXAFS data for three different sizes of Co nanoparticles sealed in the dry-box. As can be seen from Fig. 5, the FFT pattern for 12-nm nanoparticles is similar to the theoretical epsilon-Co. The ripples in the low R range for the 12-nm nanoparticles are caused by the noise of the EXAFS data in the high $k$ region. The main features in FFT

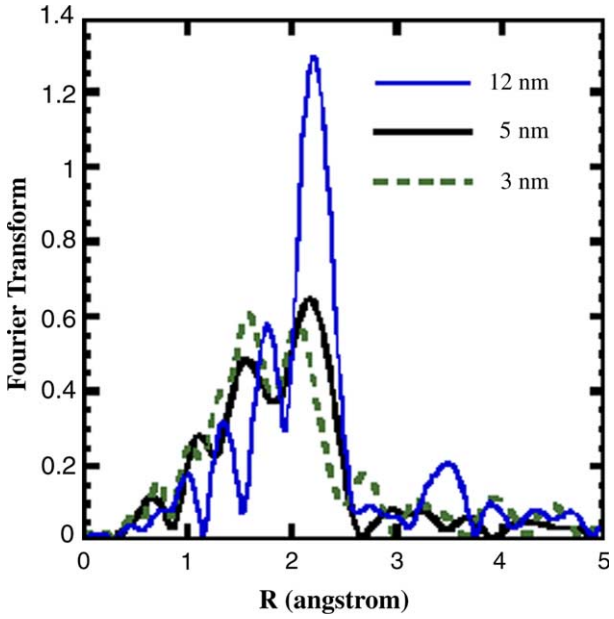


Fig. 5. Experimental EXAFS for 3, 5 and 12-nm Co nanoparticles prepared under anaerobic conditions and the corresponding Fourier transforms.

remained the same when the high $k$ noise was removed. Two peaks at 2.1 and 3.5 Å (phase uncorrected) are seen. Therefore, 12-nm nanoparticles are considered to adopt the epsilon structure, which matches the result from SAD. For 5-nm nanoparticles, two peaks at 2.2 Å (Co–Co) and 1.6 Å (Co–O) can be seen, with the Co–Co peak higher than the Co–O peak. Three-nanometer-nanoparticles also show two adjacent peaks at 2.2 and 1.6 Å, although the Co–Co peak is weaker than the Co–O peak. The oxidation could happen due to imperfect sealing of the sample holders. These results show that the smaller the nanoparticles, the more reactive they are.

However, there is a noticeable reduction to the magnitude of EXAFS patterns even for 12-nm nanoparticles in comparison with the theoretical EXAFS pattern for epsilon-Co. The first peak is filtered and fitted with Co–Co, and the best fit results are 3.36 for number of the atoms in the first shell, 2.547 Å for the radial distance, and 0.00772 for the square of Debye–Waller factor. For nanoparticles with the size of 12 nm, the surface and size effects do not have a large impact on the EXAFS patterns [26]. On the basis of TEM and EXAFS results, 12-nm nanoparticles adopt epsilon structure, which means they are crystalline and possess a long range ordering. However, the experimental EXAFS and FFT results clearly show reduced magnitudes. For instance, the first peak in FFT is reduced by 70%.

Several studies have been published concerning EXAFS investigations of nanocrystalline materials prepared by physical methods. Haubold et al. [27] reported that a 31% and 39% reduction in the Fourier transform peaks of the first and third shell for nanocrystalline fcc Cu compared to polycrystalline Cu, respectively. It was suggested that these nanocrystalline Cu structurally consists of two components with comparable volume fractions: a crystalline component and a grain boundary component, which exhibits a new solid state structure with random atomic arrange. The reduction of the signal in nanocrystalline Cu was interpreted by progressive decreasing of the effective coordination number with increasing shell number and by a wide distribution of bond length in the grain boundaries. A 52% reduction for the first shell was reported by the same group for the EXAFS studies on nanocrystalline body-centered-cubic (bcc) tungsten [28]. Sobczak and Dorozhkin [29] calculated EXAFS spectra for an Fe nanocrystal in the form of a cube of size ranging from 3 to 10 nm. However, the theoretical model calculations of grains with an ideal surface cannot explain the significant reduction of the experimental EXAFS magnitude for nanocrystalline Fe. Therefore, they have postulated a model of nanograins with a statistically disordered boundary for nanocrystalline Fe. A more severe reduction to the peak of the first shell in FFT of nanocrystalline Co was observed by Babanov et al. [30], and they suggested that the nanocrystalline Co consisted of an ordered crystalline phase and a disordered phase, and the latter was responsible for the reduction of the magnitude of the first peak in FT.

Therefore, we attribute the strong reductions of the EXAFS oscillations and Fourier transformations for our Co nanoparticles to the existence of the disordered phase (or boundary) in the nanocrystalline structure. A high-temperature annealing process may help reduce the disorder, and improve the EXAFS and Fourier transformation signal strength.

## 5. Conclusions

XAS, TEM, and AFM have been used to characterize three different sizes of Co nanoparticles synthesized by the thermo-decomposition method. TEM and AFM show that Co nanoparticles have average diameters of roughly 3, 5, and 12 nm, respectively. Electron diffraction data indicate that 12-nm nanoparticles adopt long-ranged ordering in the form of epsilon-Co structure. EXAFS has shown to be able to differentiate the epsilon from fcc and hcp. The experimental measurements of XAS spectra for three different sizes of Co nanoparticles have shown that the smaller the nanoparticles are, the more reactive they are. The existence of the disorder phase (or boundary) in the nanocrystalline structure may cause sharp decreases in the EXAFS patterns and Fourier transformations for Co nanoparticles.

## Acknowledgements

We thank the National Science Foundation (CHE 0135132) the Camille and Dreyfus Foundation for their financial supports. We thank the excellent staff at Stanford Synchrotron Radiation Laboratory (SSRL) for experimental support. We are grateful to DOE for support of the facility.

## References

[1] Z.L. Wang (Ed.), Characterization of Nanophase Materials, Wiley–VCH, Weinheim, 1999.
[2] A.S. Edelstein, R.C. Cammarata (Eds.), Nanomaterials: Synthesis, Properties and Applications, Institute of Physics Publishing, Bristol, 1998.
[3] J.H. Sinfelt, Bimetallic Catalysts: Discoveries, Concepts, and Applications, Wiley, New York, 1983.
[4] A.I. Frenkel, C.W. Hills, D. Johnson, R.G. Nuzzo, J. Phys. Chem. B 105 (2001) 12689.
[5] G. Cheng, T. Guo, J. Phys. Chem. B 106 (2001) 5833.
[6] M.S. Nashner, A.I. Frenkel, D. Somerville, C.W. Hills, J.R. Shapley, R.G. Nuzzo, J. Am. Chem. Soc. 120 (1998) 8093.
[7] C.W. Hills, M.S. Nashner, A.I. Frenkel, J.R. Shapley, R.G. Nuzzo, Langmuir 15 (1999) 690.
[8] P.N. Floriano, C.O. Noble, J.M. Schoonmaker, E.D. Poliakoff, R.L. McCarley, J. Am. Chem. Soc. 123 (2001) 10545.
[9] G. Apai, J.F. Hamilton, J. Stöhr, A. Thompson, Phys. Rev. Lett. 43 (1979) 165.
[10] D.C. Koningsberger, R. Prins (Eds.), X-ray Absorption: Principles, Applications, Techniques of EXAFS, SEXAFS, XANES, Wiley, New York, 1988.
[11] E.E. Koch (Ed.), Handbook on Synchrotron Radiation, vol. 1, North-Holland, New York, 1983.
[12] J. Rockenberger, L. Tröger, A. Kornowski, T. Vossmeyer, A. Eychmüller, J. Feldhaus, H. Weller, J. Phys. Chem. B 101 (1997) 2691.
[13] M.A. Marcus, L.E. Brus, C. Murray, M.G. Bawendi, A. Prasad, A.P. Alivisatos, Nanostruct. Mater. 1 (1992) 323.
[14] S. Davis, A. Chadwick, J. Wright, J. Phys.Chem. B 101 (1997) 9901.
[15] T. Ressler, S.L. Brock, J. Wong, S.L. Suib, J. Phys. Chem. B 103 (1999) 6407.
[16] S. Hwang, J. Choy, J. Phys. Chem. B 107 (2003) 5791.
[17] T. Shido, R.J. Prins, Phys. Chem. B 102 (1998) 8426.
[18] R.E. Benfield, D. Grandjean, M. Kröll, R. Pugin, T. Sawitowski, G. Schmid, J. Phys. Chem. B 105 (2001) 1961.
[19] D. Zanchet, H. Tolentino, M.C. Alves, O.L. Alves, D. Ugarte, Chem. Phys. Lett. 323 (2000) 167.
[20] V.F. Puntes, K.M. Krishnan, A.P. Alivisatos, Science 291 (2001) 2115.
[21] V.F. Puntes, D. Zanchet, C. Erdonmenz, A.P. Alivisatos, J. Am. Chem. Soc. 124 (2002) 12874.
[22] Available from: <http://www-ssrl.slac.stanford.edu/exafspak.html>.
[23] Available from: <http://leonardo.phys.washington.edu/feff/>.
[24] Available from: <http://feff.phys.washington.edu/~ravel/software/atoms/aboutatoms.html>.
[25] D.P. Dinega, M.G. Bawendi, Angew. Chem., Int. Ed. Engl. 38 (1999) 1788.
[26] A. Jentys, Phys. Chem. Chem. Phys. 1 (1999) 4059.
[27] T. Haubold, R. Birringer, B. Lengeler, H. Gleiter, Phys. Lett. A 135 (1989) 461.
[28] T. Haubold, W. Krauss, H. Gleiter, Philos. Mag. Lett. 63 (1991) 245.
[29] E. Sobczak, D.D. Dorozhkin, J. Alloys Comp. 286 (1999) 108.
[30] Y. Babanov, I.V. Golovshchinkova, F. Boscherini, T. Haubold, S. Mobilio, Physica B 208 and 209 (1995) 140.